Ab Initio Molecular Dynamics Study of the Solvated $OHCl^-$ Complex: Implications for the Atmospheric Oxidation of Chloride Anion to Molecular Chlorine

Raffaella D'Auria,*,† I.-F. William Kuo,‡ and Douglas J. Tobias†

Department of Chemistry and AirUCI, University of California, Irvine, Irvine, California 92697-2025, and Computational Chemical Biology, Lawrence Livermore National Laboratory, P.O. Box 808, Livermore, California 94551

Received: September 24, 2007; Revised Manuscript Received: March 11, 2008

We have studied the $OHCl^-$ complex in a six-water cluster and in bulk liquid water by means of Born−Oppenheimer molecular dynamics based on generalized gradient-corrected BLYP density functional theory. Self-interaction-corrected results, which predict a hydrogen-bonded $OH\cdots Cl^-$ complex, are compared to the uncorrected results, which predict a hemibonded $(HO—Cl)^-$. A second-order Møller−Plesset potential energy landscape of the gas-phase complex in its ground-state was computed to determine which of the two configurations represents the true nature of the complex. Because no evidence of a local minimum was found in the vicinity of the geometry corresponding to $(HO—Cl)^-$, we conclude that the self-interaction-corrected results are more accurate and, therefore, that the complex is held together by a hydrogen-bond-like interaction in both an asymmetric solvation environment, as represented by the cluster, and a symmetric solvation environment, as represented by the bulk system. We postulate that the mechanism that governs the atmospheric oxidation of $Cl^-(aq)$ to $Cl_2(g)$ on the surface of marine aerosols is initiated by the formation of a H-bonded $OH\cdots Cl^-$ complex. Furthermore, because no evidence of charge transfer from Cl^- to OH was found, in either the liquid or the cluster environment, we propose that the second step of the oxidation of Cl^- is the reaction of the complex with a second Cl^-, resulting in the formation of the species Cl_2^- and OH^-. $Cl_2(g)$ could then be formed via an electron-transfer reaction with an impinging OH molecule.

Introduction

The interaction of chloride anion with water and ȮH has been the subject of several experimental[1–4] and theoretical[4] investigations. Jayson et al.[1] conducted a series of pulse radiolysis experiments of aqueous sodium chloride solutions and interpreted their results on the basis of the following sequence of reactions

$$OH + Cl^- \rightarrow ClOH^- \quad (1)$$

$$ClOH^- + H^+ \rightarrow \dot{Cl} + H_2O \quad (2)$$

$$Cl + Cl^- \rightarrow Cl_2^- \quad (3)$$

where the equilibria in eqs 1 and 2 are shifted to the left at low Cl^- concentration and at low acidity levels, respectively. Operating at low acidity and high chloride concentration, Jayson and co-workers recorded an electronic absorption spectra peaked at 350 nm, which they attributed to a $ClOH^-$ species. In an electron spin resonance (ESR) study of γ-irradiated hydrates of $BaCl_2$, Catton and Symons[3] identified a species that they assigned as the $ClOH^-$ radical. They estimated the spin density on the chlorine atom to be either 0.288 or 0.466, where the second value would confirm a complex with a shared electron. Sevilla et al.[4] also collected electron spin resonance spectra after γ-irradiation of a series of frozen aqueous solutions containing Cl^-. Upon annealing of the samples from 77 to 125 K, they consistently detected a "stepwise development of the ESR signal of a Ċl—X species" accompanied by a decrease in the ȮH signal. Sevilla and coworkers attributed the observed ESR Ċl—X signal to the $\dot{C}l—OH_2$ complex rather than the $\dot{C}l—OH^-$ species, because their experiments were run under low-pH conditions. They pointed out, however, that the intermediate complex, formed as a result of the attack of the hydroxyl radical on the chloride anion, should be a chloride−hydroxyl radical complex. A companion theoretical investigation of the interaction of chloride ions and hydroxyl radicals, as well as the interaction between the chlorine atom and water, was carried out by Sevilla et al. At the different levels of theory employed in the electronic structure calculations (including uMP2/6-31+G* and PM3), the authors noted that the equilibrium structure for the gas-phase chloride ion−hydroxyl radical complex (with and without water) always has the hydroxyl hydrogen oriented toward the Cl^-. The $OHCl^-$ complex has also been studied in the gas phase by Neumark and coworkers.[5] In their work, a comparison of measured and computed photodetachment spectra of $OHCl^-$ was presented. The structure of the complex was determined to be the linear, hydrogen-bonded species $OH\cdots Cl^-$.

The collection of work summarized above suggests that, depending on the solvation environment, the complex can assume two different structures: covalently bonded $\dot{C}lOH^-$ [1,3] and H-bonded $OHCl^-$.[5] The chemistry of chloride ions and OH radicals in an aqueous environment (as well as in the gas phase) is an intriguing problem whose investigation poses challenges from both the computational and experimental points of view. In atmospheric chemistry, the interactions between the two species are eventually responsible for the oxidation of chloride ions present, for example, in marine aerosol[6] to gaseous Cl_2, which, in urban environments, is a precursor of ozone, a dangerous tropospheric pollutant. A sound understanding of the fundamental chemistry involved in this oxidation process is

* To whom correspondence should be addressed. E-mail: rdauria@uci.edu.
† University of California, Irvine.
‡ Lawrence Livermore National Laboratory.

10.1021/jp077669d CCC: $40.75
Published on Web 04/29/2008

required to understand and predict the production and fate of tropospheric O_3. In particular, marine aerosols, present in coastal regions, have been found to be a source of atmospheric molecular chlorine in the presence of an airborne oxidative species (such as OH).[7] Heterogeneous chemistry has been invoked to explain the molecular chlorine yields observed in an aerosol chamber study.[8] Classical molecular dynamics studies have shown that a substantial population of chloride anions is found at the particle interface[9] and that OH accumulates at the air−particle interface,[10] making the formation of a reactive $OH\cdots Cl^-$ complex possible (and indeed observed in molecular dynamics simulations of OH radicals impinging on a NaCl aqueous solution).[11] The proposed mechanism[8] for the oxidation of adsorbed Cl^- at the particle interface to gaseous Cl_2 goes through the following steps:

$$Cl^-(\text{int}) + OH(g) \rightarrow (OH\cdot\cdot Cl^-)(\text{int}) \quad (4)$$

$$2(OH\cdot\cdot Cl^-)(\text{int}) \rightarrow Cl_2(g) + 2OH^-(aq) \quad (5)$$

where the label int denotes an interfacial species. The first step of this mechanism, reaction 4, requires the formation of an $OH\cdots Cl^-$ complex as a result of the interaction between gaseous OH radicals impinging on the aerosol interface and an interfacial chloride anion. Roeselová et al.[10] computed the expected interfacial OH concentration to be around 2.3×10^{10} radicals/cm^3. Considering a coarse marine aerosol particle of 1 μm radius, the number of OH radicals on such a particle would then be ca. 0.1. Thus, the likelihood of two such complexes colliding, according to reaction 5, is expected to be extremely low. Another possibility is that reaction 5 could be replaced by

$$(OH\cdot\cdot Cl^-)(\text{int}) + Cl^-(\text{int}) \rightarrow Cl_2^-(\text{int}) + OH^-(aq) \quad (6)$$

$$Cl_2^-(\text{int}) + OH(g) \rightarrow Cl_2(g) + OH^-(aq) \quad (7)$$

Alternatively, reactions 4 and 5 could be replaced by

$$Cl^-(\text{int}) + OH(g) \rightarrow Cl(\text{int}) + OH^-(aq) \quad (8)$$

$$Cl^-(\text{int}) + Cl(\text{int}) \rightarrow Cl_2^-(\text{int}) \quad (9)$$

$$Cl_2^-(\text{int}) + OH(g) \rightarrow Cl_2(g) + OH^-(aq) \quad (10)$$

Reaction 8 is energetically uphill in the gas phase because the electron affinity of Cl is 1.78 eV larger than that of OH.[12,13] A comparison of the redox potentials for the Cl/Cl^- and OH/OH^- couples (+2.6 and +1.9 V, respectively)[14] reveals that, even in an aqueous environment, the reaction would likely still be unfavorable.

To elucidate the possible reaction mechanism and to understand the nature and role of the chloride−hydroxyl radical complex, we performed a series of ab initio molecular dynamics simulations on two analogous systems: a six-water $Cl^-H\dot{O}$ cluster and a bulk-like system containing 57 water molecules, one Cl^- anion, and one $\dot{O}H$ radical with three-dimensional periodic boundary conditions. The first system was designed to mimic an asymmetric solvation environment such as an interface, whereas the second was devised to understand the role of a symmetric solvation environment. Our results suggest that the oxidation mechanism does proceed through the formation of a chloride−hydroxyl radical complex and that, therefore, reaction 4 occurs. We also found that, for this class of open-shell system, particular care has to be taken when using a density functional theory (DFT) variant of ab initio molecular dynamics, as in the current study, to ensure that self-interaction error[15] (SIE) is taken into account. Although the issue of SIE has been well-known to the community for many years,[16] it has recently resurfaced and been addressed in different studies.[17–20] In this work, we compare results obtained when a straightforward DFT method is adopted and when an SIE-corrected version is implemented. We believe that such a comparison is timely and much needed in view of the increasing use of DFT-based molecular dynamics.

Computational Details

Ab initio molecular dynamics simulations were carried out for a representative cluster and bulk system for 20 ps with a time step of 0.48 fs. The cluster simulations, which included one chloride anion, one hydroxyl radical, and six water molecules, were performed in the microcanonical (NVE) ensemble and employed cluster boundary conditions.[21] The bulk simulations, which contained one chloride anion, one hydroxyl radical, and 57 water molecules in a cubic box of edge length 13 Å with three-dimensional periodic boundary conditions, were performed in the canonical ensemble (NVT) using one Nosé−Hoover thermostat for every degree of freedom with a characteristic frequency of 2000 cm^{-1}. The interaction potential employed was based on the restricted open-shell Kohn−Sham formulation of density functional theory, as implemented in the open-source simulation package CP2K.[22] The electronic structure was explicitly quenched at every time step to a tolerance of 1.0×10^{-7} to conserve energy.

The electronic structure was computed via the QuickStep module in the CP2K simulation package.[22,23] QuickStep uses a dual basis set formalism of Gaussian-type orbitals (TZV2P) and plane waves expanded to a 280 Ry cutoff for the density.[24] With the use of plane waves, GTH (Goedecker–Teter–Hutter)[25] pseudopotentials were employed to describe the core−electronic states. The exchange and correlation (XC) energies were described using the BLYP functionals.[26,27] All calculations were carried out within the restricted open-shell formalism. We performed each simulation with and without the self-interaction correction (SIC) scheme of VandeVondele and Sprik.[18] The associated scaling parameter used for the singly occupied orbital for the Hartree energy was 0.2, and the approximate XC parameter was set to 0.0. This set of parameters was shown to provide a good compromise between localized and delocalized spin density.[18] The temperature of the bulk simulations, both with and without the SIC, were kept at 300 K by the thermostats. The average temperatures of the clusters simulated with and without the SIC were ∼150 and ∼200 K, respectively.

A single-point uMP2/aug-cc-pVDZ computation was performed for the six-water cluster system in the $HOCl^-$ configuration to check for the presence of bonding orbitals. In addition, a potential energy surface (PES) scan was computed for the gas-phase $OHCl^-$ complex at the same level of theory to investigate whether the $HOCl^-$ arrangement corresponds to a local minimum. The scan was performed while varying the Cl−O distance and the Cl−O−H angle but keeping the O−H distance fixed at 1 Å. All of the uMP2 calculations were carried out using the Gaussian 98[31] suite of programs.

Results and Discussion

$(HO-Cl)^-$ versus Hydrogen-Bonded $OH\cdots Cl^-$. Two main chloride anion−hydroxyl radical complex structures were identified in the simulations. In the standard DFT simulations, without the SIC, the complex appears in a $(ClOH)^-$ configuration. Analysis of its structure in terms of geometry and by location of the Wannier function centers (WFCs)[28] (vide infra) indicates that, in the cluster, as well as in the bulk case, the complex is held together by a Cl−O bond. This bond appears

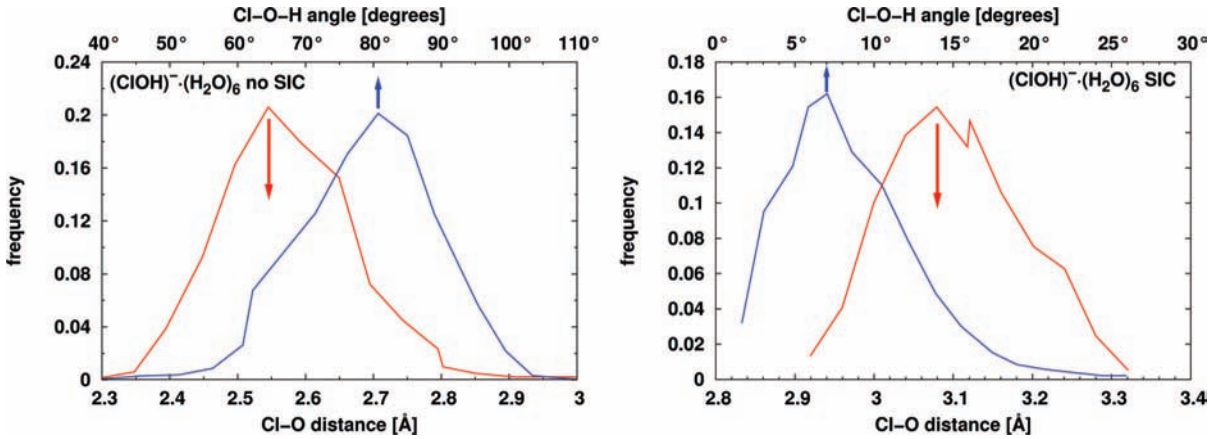

Figure 1. Histograms of the Cl—O distance and the Cl—O—H angle for the $Cl^- \cdots H\dot{O}$ complex in a six-water cluster obtained from simulations without (left) and with (right) the self interaction correction.

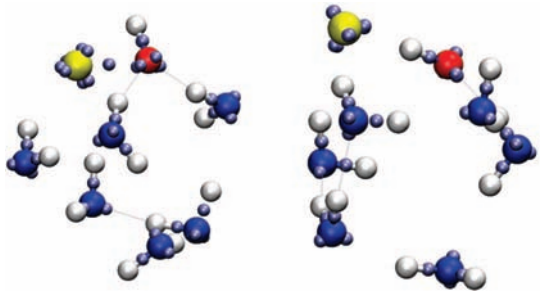

Figure 2. Hemibonded $(ClOH)^- \cdot (H_2O)_6$ (left) and H-bonded $OHCl^- \cdot (H_2O)_6$ (right) cluster geometries observed in simulations without and with the SIC, respectively. Water oxygens are depicted in blue, OH oxygen in red, hydrogens in white, and chlorine in yellow, and the gray spheres represents the WFCs (see text).

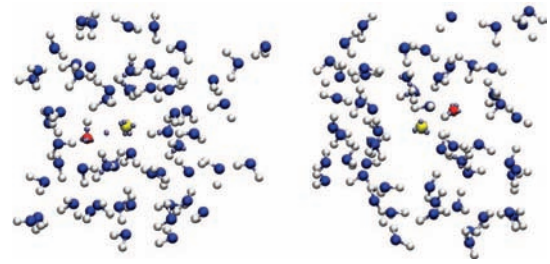

Figure 3. Hemibonded $(ClOH)^-$ (left) and H-bonded $OHCl^-$ (right) configurations of the complex between Cl^- and OH radical in bulk aqueous solution from simulations without and with the SIC, respectively. Only the WFCs within 4 Å of the chlorine are shown. The coloring scheme is as in Figure 2.

to be a three-electron bond (hemibond) between the partially occupied oxygen orbital and one lone pair of the chloride ion. In the SIE-corrected DFT simulations, the complex was found, for the most part, to be in a linear $OHCl^-$ configuration and, therefore, to be H-bonded.

In Figure 1, the histograms of the Cl—O distance and the Cl—O—H angle are shown for the cluster simulations without (left) and with (right) the SIC. In the case when the SIC is not included, the Cl—O—H angle ranges around 80°, and the histogram of the Cl—O distance has a peak around 2.5 Å. When the SIC is included, the histogram of the Cl—O—H angle peaks around 7°, and the Cl—O most probable distance lies around 3 Å.

In Figure 2, snapshots of the six-water cluster obtained by DFT simulations without and with the SIC are shown. In Figure 3, analogous snapshots are shown for the bulk simulations.

In the snapshots, the atoms are shown together with the centers of their maximally localized Wannier functions.[29] The maximally localized Wannier functions are analogous to localized molecular orbitals obtained by transformation of the original delocalized Kohn—Sham orbitals. The centers represent the positions of the maximum probability of finding an electron.[30] The Wannier function centers (WFCs) are thus useful for monitoring the positions where the excess negative charge is likely to be found. In the case of the standard (no SIC) DFT results, shown in the left panels of Figures 2 and 3, the position of maximum probability for the extra electron appears to be between the chlorine atom and the hydroxyl oxygen, in line with what could be expected for a hemibond-like interaction. In the SIE-corrected simulations, the negative charge appears to be localized on the chlorine atom. In the simulations without the SIC, the average distances between the shared WFC and the chlorine atom or hydroxyl radical oxygen are about 1 Å.

To further characterize the nature of the two observed complexes, in Figure 4, we present a Mulliken analysis of the six-water cluster DFT and SIC-DFT simulations to understand how the charge and spin are partitioned in the two cases. In the covalently bonded structure, the excess negative charge is roughly equally split between the Cl and the O atoms, and the density of spin is concomitantly smeared among the two species, in accordance with what could be expected of a hemibonded interaction. In the SIC-DFT results, where the complex is H-bonded, the excess charge is mostly centered on the chlorine, whereas the spin is concentrated on the oxygen, as expected.

Kinetic Stability of the $Cl^- \cdots H\dot{O}$ Complex. To illustrate the degree to which the OH and Cl^- were complexed throughout the simulations, we show plots in Figure 5 of the time evolution of various internal degrees of freedom of the complex, specifically, the Cl—O, O—H, and Cl—H distances and the Cl—O—H angle.

The results for the DFT and SIC-DFT simulations of the complexes in the six-water clusters, displayed in the top panels of Figure 5, show that the complex is fairly stable in a cluster environment, at least on the 20-/15-ps time scale. The complex is also stable in the standard (no SIC) DFT bulk simulation, shown in the bottom left panel of Figure 5. In the SIE-corrected bulk simulation of $ClOH^-$, shown in the bottom right panel of Figure 5, the complex is more labile, appearing to break and reform on the time scale of picoseconds.

To elucidate the solvation in the latter case, we show plots in Figure 6 of the radial distribution functions of the water oxygens and the water hydrogens about Cl^- (left) and the radii of the solvation shell of water oxygens and hydrogens

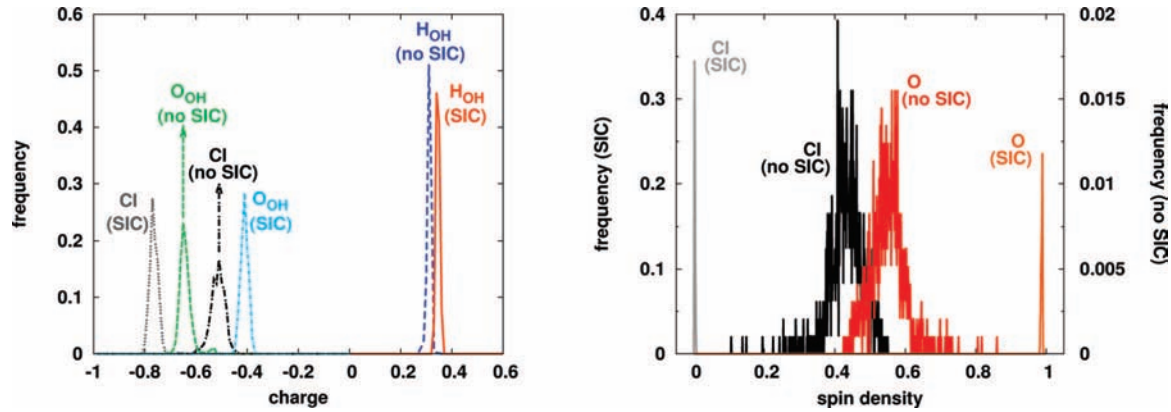

Figure 4. Histograms of the charge (left) and spin density (right) distributions obtained by a Mulliken analysis performed on the standard DFT and SIC-DFT six-water cluster trajectories. In the standard DFT case, the charge and spin densities are largely shared between the oxygen of the hydroxyl radical and the chlorine anion. In the SIC-DFT case, the net excess charge is largely concentrated on the chlorine, whereas the spin density is mostly concentrated on the oxygen.

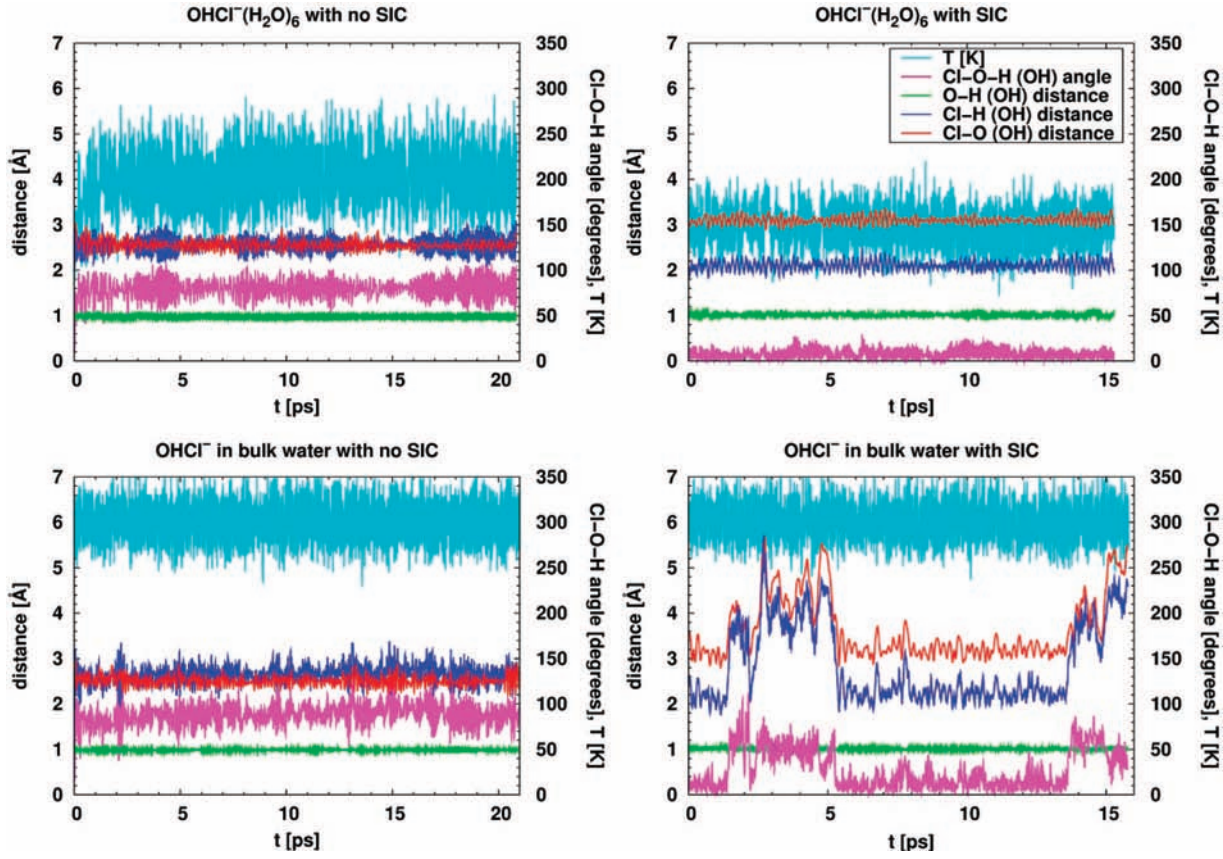

Figure 5. Time evolution of the geometrical parameters characterizing the complex (i.e., Cl—O distance, O—H distance, Cl—H distance, and Cl—O—H angle).

around the chloride ion (right). On the time scale of our simulations, the hydroxyl radical is always contained well within the water second solvation shell about the chloride ion. Although this feature could be due to the restricted size of the fundamental simulation box (13 × 13 × 13 Å), which does not extend beyond the water second solvation shell around the chloride ion, the chloride-to-hydroxyl distance is never observed to become larger than the position of the second peaks in the radial distribution functions (corresponding to the second chloride—water solvation shell). Incidentally, the size of the periodic box produces a situation analogous to a concentrated solution, where another chloride ion would be found in the vicinity of the first.

It should be noted that the results of the Mulliken analysis included in Figure 4 do not show a tendency of any of the systems to undergo a charge exchange. Therefore, given the degree of stability observed for the chloride—hydroxyl radical complex in all four cases considered and the localization of the charge in both cluster simulations (with and without the SIC) on the chlorine side of the complex, we conclude that the OH-induced oxidation of Cl^- begins with the formation of the chloride—hydroxyl radical complex through reaction 4.

Comparison with uMP2 Calculations. A single-point uMP2/aug-cc-pVDZ computation of the covalently bonded six-water cluster was performed to investigate whether a bonding molecular orbital could be detected. The cluster geometry on

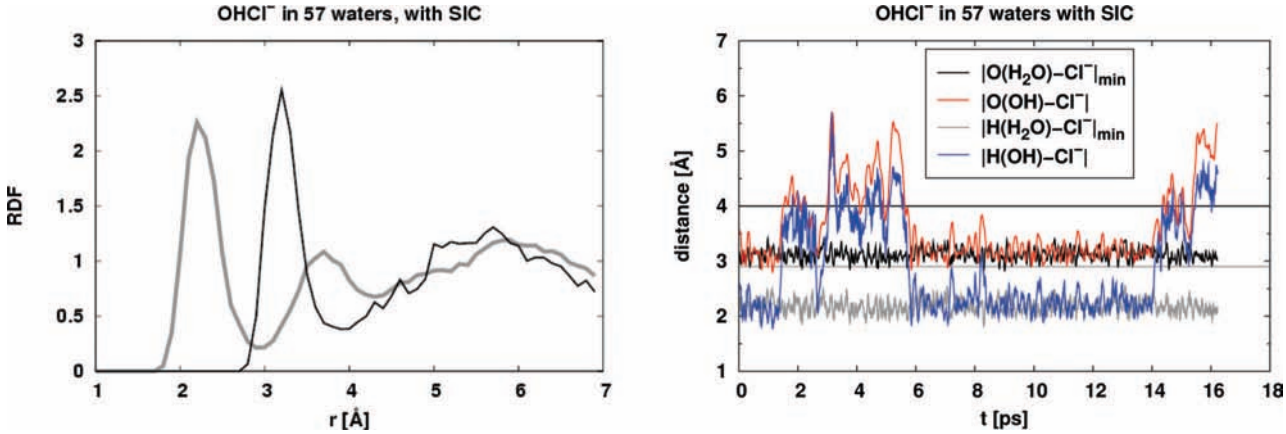

Figure 6. (Left) Radial distribution functions of H_{H_2O} (gray line) and O_{H_2O} (black line) about Cl^-. (Right) $Cl{-}H_{OH}$ and $Cl{-}O_{OH}$ distances as a function of time (blue and red lines, respectively). The black horizontal line represents the location of the first minimum in the RDF of the water oxygens around chloride, and the gray horizontal line represents the location of the first minimum in the RDF of the water hydrogens about the chloride ion (i.e., the radii of the respective first solvation shells).

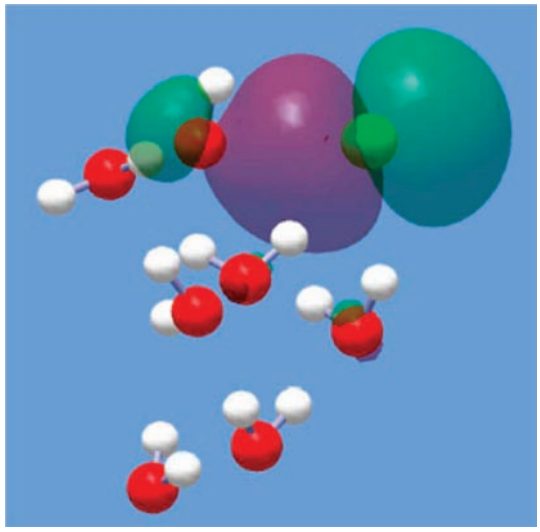

Figure 7. Hartree−Fock bonding molecular orbital for the covalently bonded $OHCl^-\cdot(H_2O)_6$ cluster obtained from a single-point uMP2/aug-cc-pVDZ computation. In the figure, the oxygen atoms are shown in red, the hydrogen atoms in white, and the chlorine atom in green.

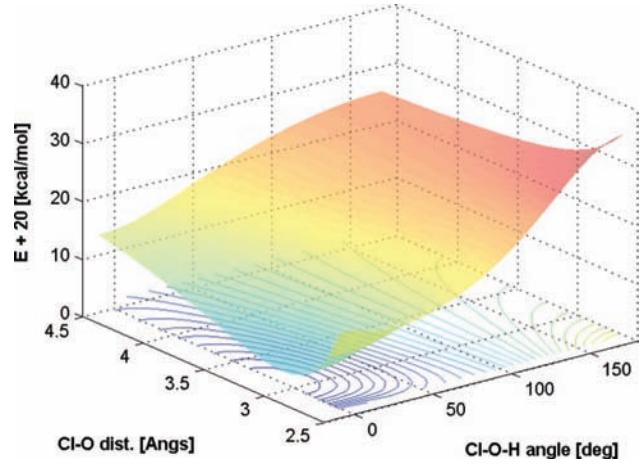

Figure 8. Scan of the potential energy surface of the $OHCl^-$ complex at the uMP2/aug-cc-PVDZ level of theory. The O−H distance was fixed at 1Å. The zero of energy corresponds to the dissociated cluster (i.e., Cl^- and OH).

which the computation was performed, is a snapshot of the corresponding molecular dynamics simulation without the SIC. A bonding orbital was indeed found and is displayed in Figure 7.

To clarify the nature of the $OHCl^-$ complex in the gas phase, we performed a uMP2/aug-cc-pVDZ scan of the potential energy surface by varying the Cl−O−H angle and the Cl−O distance. The scan was obtained with the O−H distance held fixed at 1 Å while the Cl−O distance and Cl−O−H angle were varied. The global energy minimum of the resulting potential energy surface, shown in Figure 8, corresponds to the H-bonded complex (Cl−O distance = 3.1 Å, Cl−O−H angle = 0°). In contrast, the covalently bonded structure, observed in the SIE-uncorrected DFT simulations of the complex in a six-water cluster and in bulk water, corresponds to a point on the PES of the gas-phase complex (Cl−O = 2.6 Å and Cl−O−H = 80°) where no minimum is present. In Figure 9, we present a comparison of the potential energy curves as a function of the chlorine-to-oxygen distance for the gas-phase complex (for O−H = 1 Å and Cl−O−H = 0° or 80°) obtained at the uMP2/aug-cc-pVDZ with the standard BLYP and with SIC-BLYP methods. Although both DFT computations predict energy minima at Cl−O distances (for both the linear and bent structures) that agree with the uMP2/aug-cc-pVDZ computation. The results for the SIE-uncorrected DFT computations strongly overestimate the depth of the minima and predict that the bent complex is slightly more energetically stable than the linear complex. (Note that, for the bent structure, the PES shows a minimum only along the Cl−O coordinate; when the Cl−O−H angle is also varied, there is no minimum about the Cl−O ≈ 2.6 Å and Cl−O−H ≈ 80° geometry.) The standard DFT computations underestimate the binding energy of the complex in either geometry because of excessive spin delocalization. The spin is largely delocalized in the geometry predicted by the standard BLYP method corresponding to the bent structure (the spin on the oxygen atom is 0.5 for the Cl−O distances of 2.0 and 2.2 and increases to ∼0.7 for the longer values of the Cl−O distance, while the spin on Cl goes from ∼0.5 to 0.3), thus determining the considerable 15 kcal/mol deviation in the binding energy with respect to the uMP2/aug-cc-pVDZ estimate. The spin is also moderately delocalized in the H-bonded SIC-BLYP complex (the spin delocalization roughly increases as the Cl−O distance increases: the spin on O is ∼0.9 at 2.6 Å and ∼0.8 at 3.8 Å), thus giving rise to the difference in the binding energy of about 5 kcal/mol compared to the uMP2/aug-cc-pVDZ computation. In Table 1, the geometries and energies at which the potential energy curves experience minima

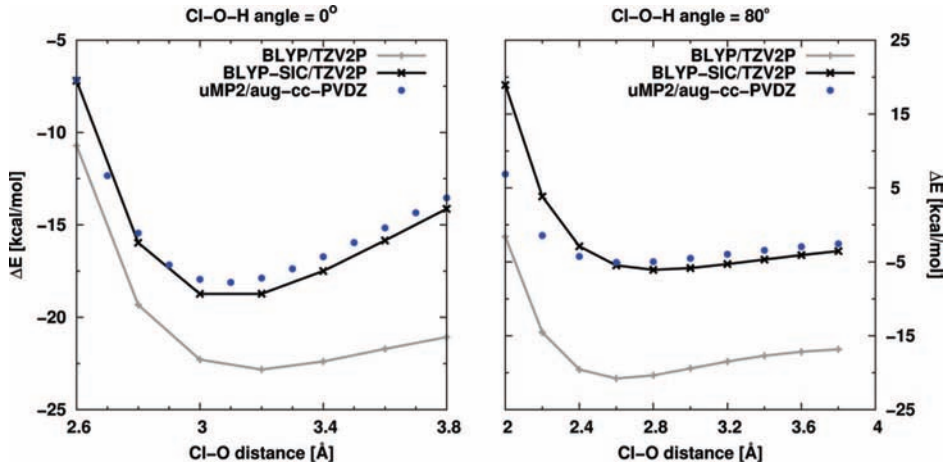

Figure 9. Comparison of the PES scan along Cl—O—H angles of 0° and 80° for the different computations. The zero of energy corresponds to the dissociated cluster (i.e., Cl^- and OH).

TABLE 1: Position of the Minimum in the Potential Energy Curve with Respect to the Cl—O Distance and Corresponding Energies Obtained by the Different Methods[a]

	Cl—O distance (Å), energy (kcal/mol)		
Cl—O—H angle (deg)	uMP2/ aug-cc-pVDZ	BLYP/ TZV2P	SIC-BLYP/ TZV2P
0	3.1, −18.1	3.2, −22.8	3.0, −18.7
80	2.6, −5.1	2.6, −20.8	2.8, −6.1

[a] Note that, for the Cl—O—H angle equal to 80°, the minimum on the curve does not correspond to a minimum on the PES (see Figure 8).

are summarized. The favorable comparisons of the gas-phase results with the uMP2/aug-cc-pVDZ values seem to indicate that our SIC-BLYP results for the hydrated $OHCl^-$ species are correct and that SIC-BLYP is viable technique for open-shell systems. In contrast, unphysical conclusions are reached when the standard BLYP method is used without any correction for the self-interaction error.

Extrapolating the results obtained for the gas-phase complex to the results obtained for the six-water cluster and the bulk system, we conclude that the observed covalently bonded complex in the SIE-uncorrected BLYP computations represents a failure of the computational technique. On the other hand, the results obtained with the SIE-corrected DFT technique appear to describe the complex accurately and consistently as being hydrogen-bonded.

Conclusions

This article describes results from an ab initio molecular dynamics study of the chloride ion—hydroxyl radical complex in asymmetric (cluster) and symmetric (bulk) solvation environments. The complex appears to exist in two different configurations depending on whether a standard (no self-interaction correction) or self-interaction-corrected BLYP DFT scheme is employed. We compared results obtained with the two DFT schemes to a uMP2/aug-cc-pVDZ scan of the ground-state energy landscape of the complex in the gas phase. The absence of a local minimum in the vicinity of the geometry predicted by the uncorrected DFT results is taken as evidence that standard DFT techniques fail to capture the correct geometry of open-shell systems, such as the one under consideration, because of the presence of the self-interaction error. On the other hand, SIE-corrected BLYP results appear to be able to predict the correct behavior (assuming that the uMP2 reults are correct) of the open-shell system considered here. The SIE correction scheme that we used has been already shown to yield results for the OH—water system that are in good agreement with high-level ab initio computations.[18] Regarding the oxidation of Cl^-(int) to Cl_2(g), we conclude that, because no evidence of charge transfer between Cl^- and OH is observed in either the cluster or bulk system, the reaction most likely begins with the formation of the H-bonded $OHCl^-$ complex that proceeds to react with a second Cl^- to form Cl_2^-, which is subsequently oxidized by a second OH radical. We note that the electrostatic repulsion between the two negative centers could conceivably be surmounted by crowding of chloride anions and the presence of counterions at the interface of concentrated sodium chloride aqueous solutions, as revealed by classical molecular dynamics simulations.[9]

Acknowledgment. We are grateful to the anonymous reviewers for comments that helped us improve the manuscript. This work was supported by the AirUCI Environmental Molecular Sciences Institute under Grants CHE043312 and CHE0209719 from the National Science Foundation. Part of this work was performed under the auspices of the U.S. Department of Energy by University of California LLNL under Contract W-7405-Eng-48. Computer resources were provided by the airuci cluster at UCI and Livermore Computing at LLNL.

References and Notes

(1) Jayson, G. G.; Parsons, B. J.; Swallow, A. J. *J. Chem. Soc., Faraday Trans.* **1973**, *69*, 1597–1607.
(2) Treinin, A.; Hayon, E. *J. Am. Chem. Soc.* **1975**, *97*, 1716–1721.
(3) Catton, R. C.; Symons, M. C. R. *J. Chem. Soc. A.* **1969**, 446–451.
(4) Sevilla, M. D.; Summerfield, S.; Elizer, I.; Rak, J.; Symons, M. C. R. *J. Phys. Chem. A* **1997**, *101*, 2910–2915.
(5) Davis, H.; Koizumi, M. J.; Schatz, G. C.; Bradforth, S. E.; Neumark, D. M. *J. Chem. Phys.* **1994**, *101*, 4708–4721.
(6) Marine aerosols, or sea salt aerosols, are atmospheric particles mostly generated by the mechanism of bubble bursting. Whereas their initial composition should resemble that of sea water, as the particles enter the atmosphere, the water evaporates (to allow the aerosol particle to equilibrate), and the particle composition becomes generally close to that of deliquesced or saturated salt solutions.
(7) Spicer, C. W.; Chapman, E. G.; Finlayson-Pitts, B. J.; Plastridge, R. A.; Hubbe, J. M.; Fast, J. D.; Berkowitz, C. M. *Nature* **1998**, *394*, 353–356.
(8) Knipping, E. M.; Lakin, M. J.; Foster, K. L.; Jungwirth, P.; Tobias, D. J.; Gerber, R. B.; Dabdub, D.; Finlayson-Pitts, B. J. *Science* **2000**, *288*, 301–306.
(9) Jungwirth, P.; Tobias, D. J. *J. Phys. Chem. B* **2000**, *104*, 7702–7706.

(10) Roeselová, M.; Vieceli, J.; Dang, L. X.; Garrett, B. C.; Tobias, D. J. *J. Am. Chem. Soc.* **2004**, *126*, 16308–16309. For details on the computation of the interfacial concentration of OH, see the article's Supporting Information.

(11) Roeselova, M.; Jungwirth, P.; Tobias, D. J.; Gerber, R. B. *J. Phys. Chem. B,* **2003**, *107*, 12690–12699.

(12) Schulz, P. A.; Mead, R. D.; Jones, P. L.; Lineberger, W. C. *J. Chem. Phys.* **1982**, *77*, 1153–1165.

(13) Trainham, R.; Fletcher, G. D.; Larson, D. J. *J. Phys. B: At. Mol. Opt. Phys.* **1987**, *20*, L777–L784.

(14) NDRL (Notre Dame Radiation Laboratory) Radiation Chemistry Data Center, http://www.rcdc.nd.edu/.

(15) Koch, W.; Holthausen, M. C. *A Chemist'S Guide to Density Functional Theory*; Wiley-VCH Verlag GmbH: Weinheim, Germany, 2001; pp 85−88.

(16) Zunger, A.; Perdew, R. J.; Oiver, G. L. *Solid State Commun.* **1980**, *34*, 933–936.

(17) d'Avezac, M.; Calandra, M.; Mauri, F. *Phys. Rev. B* **2005**, *71*, 205210-1–205210-5.

(18) VandeVondele, J.; Sprik, M. *Phys. Chem. Chem. Phys.* **2005**, *7*, 1363–1367.

(19) Runzsinszky, A.; Perdew, J. P.; Csonka, G. I.; Vydrov, O. A.; Scuseria, G. *J. Chem. Phys.* **2007**, *126*, 104102-1–104102-8.

(20) Cohen, A. J.; Mori-Sánchez, P.; Yang, W. *J. Chem. Phys.* **2007**, *textit126*, 191109-1–191109-5.

(21) Martyna, G. J.; Tuckerman, M. E. *J. Chem. Phys.* **1999**, *110*, 2810–2821.

(22) *CP2K*; CP2K Developers Group, 2007; http://cp2k.berlios.de/.

(23) VandeVondele, J.; Krack, M.; Mohamed, F.; Parrinello, M.; Chassaing, T.; Hutter, J. *Comput. Phys. Commun.* **2005**, *167*, 103–128.

(24) Lippert, G.; Hutter, J.; Parrinello, M. *Mol. Phys.* **1997**, *92*, 477–488.

(25) Goedecker, S.; Teter, M.; Hutter, J. *Phys. Rev. B* **1996**, *54*, 1703–1710.

(26) Becke, A. D. *J. Chem. Phys.* **1993**, *98*, 5648–5652.

(27) Lee, C.; Yang, W.; Parr, R. G. *Phys. Rev. B* **1988**, *37*, 785–789.

(28) Berghold, G.; Mundy, C. J.; Romero, A. H.; Hutter, J.; Parrinello, M. *Phys. Rev. B* **2000**, *61*, 10040–10048.

(29) Wannier, G. H. *Phys. Rev.* **1937**, *52*, 191–197.

(30) Marzari, N.; Vanderbilt, D. *Phys. Rev. B* **1997**, *56*, 12847–12865.

(31) Frisch, M. J.; Trucks, G. W.; Schlegel, H. B.; Scuseria, G. E.; Robb, M. A.; Cheeseman, J. R.; Zakrzewski, V. G.; Montgomery, J. A., Jr.; Stratmann, R. E.; Burant, J. C.; Dapprich, S.; Millam, J. M.; Daniels, A. D.; Kudin, K. N.; Strain, M. C.; Farkas, O.; Tomasi, J.; Barone, V.; Cossi, M.; Cammi, R.; Mennucci, B.; Pomelli, C.; Adamo, C.; Clifford, S.; Ochterski, J.; Petersson, G. A.; Ayala, P. Y.; Cui, Q.; Morokuma, K.; Malick, D. K.; Rabuck, A. D.; Raghavachari, K.; Foresman, J. B.; Cioslowski, J.; Ortiz, J. V.; Stefanov, B. B.; Liu, G.; Liashenko, A.; Piskorz, P.; Komaromi, I.; Gomperts, R.; Martin, R. L.; Fox, D. J.; Keith, T.; Al-Laham, M. A.; Peng, C. Y.; Nanayakkara, A.; Gonzalez, C.; Challacombe, M.; Gill, P. M. W.; Johnson, B. G.; Chen, W.; Wong, M. W.; Andres, J. L.; Head-Gordon, M.; Replogle, E. S.; Pople, J. A. *Gaussian 98*, revision A.1x; Gaussian, Inc.: Pittsburgh, PA, 1998.

JP077669D